Improvement and Uncertainties of Global Simulation of Sulfate Concentration and Radiative Forcing in CESM2

Wendong Ge[1], Junfeng Liu[1], Songlin Xiang[1], Yuhan Zhou[1], Jingcheng Zhou[1], Xiurong Hu[2], Jianmin Ma[1], Xuejun Wang[1], Yi Wan[1], Jianying Hu[1], Zhaobin Zhang[1], Xilong Wang[1], Shu Tao[1]

[1]Laboratory for Earth Surface Processes, College of Urban and Environmental Sciences, Peking University, Beijing, 100871, China

[2] College of Economics and Management, Nanjing University of Aeronautics and Astronautics, Nanjing, 211106, China

Corresponding author: Junfeng Liu (jfliu@pku.edu.cn)

Key Points:

- The global simulations of sulfate distribution and radiative forcing are significantly improved with the usage of CESM2.

- Wet deposition is the key process governing both the horizontal and vertical distributions of global sulfate concentrations.

- The uncertainty of sulfate forcing is very important to the formulation of global carbon neutral policies.

Abstract

Sulfate is a major atmospheric pollutant and radiative forcing (RF) factor that influences air quality, cloud microphysics and climate. Therefore, a better evaluation of sulfate concentrations and RF patterns is essential for policy-making and the management of air pollution and climate change. This study comprehensively estimates the global distribution of sulfate concentrations and RFs and analyzes the sources of uncertainty in the Community Earth System Model version 2 (CESM2) and the Parallel Offline Radiative Transfer (PORT) model. Compared with the observations, the incorporation of detailed in-cloud aqueous-phase chemistry and the enhanced wet deposition flux of sulfate significantly improved the simulations of sulfur species both near the ground and at high altitudes, which is beneficial for a more accurate estimation of the global sulfate RF. The improved simulated RF of sulfate from 1850 to 2015 is -0.382 W·m^{-2}. This study finds that wet deposition is the key process governing both the horizontal and vertical distributions of sulfate concentrations. The overestimation of surface sulfate and the underestimation of high-altitude sulfate made by the model are essential uncertainty factors of the sulfate RF estimation. This study emphasizes the importance of improving the simulation of global sulfate distribution as well as its RF, which may strongly pressure the near-future warming potential when witnessing a rapid transition to a carbon neutral world that is phasing out fossil fuel. A more accurate assessment of sulfate levels and radiation effects will play a remarkable guiding role in the formulation of global emission reduction-related policies in the future.

Plain Language Summary

Sulfate aerosols play an essential role in the entire atmosphere and climate system. Therefore, it is necessary to better simulate the distribution and radiative forcing of sulfate. By using a global climate model, we improved the simulation of sulfate distribution both near the ground and at high altitudes and achieved a more accurate estimation of the global radiative forcing of sulfate. We found that wet deposition is the key process influencing the distribution of sulfate concentrations. The overestimation of surface sulfate and the underestimation of high-altitude sulfate are important uncertainty factors of sulfate radiative forcing. Our results suggest that more field studies (e.g., aircraft campaigns, surface measurements over remote regions, etc.) of sulfate are urgently needed. This study indicates that large uncertainties may exist in current global climate models, which may impact the formulation of future policy-making in carbon neutrality.

1 Introduction

Sulfate is one of the major species of aerosol. Both natural sources (such as oxidation of dimethyl sulfur (DMS)) over the ocean and anthropogenic emissions of sulfur dioxide (SO_2) are important sources of sulfate (Hussain & Lun, 2019; Sanchez et al., 2018; Yan & Xu, 2021). Human industrial activities have increased significantly since the industrial era, and the gas-phase, liquid-phase and surface heterogeneous oxidations of SO_2 have gradually accounted for the main sources of sulfate (B. Liu et al., 2017; Xue et al., 2016). As an important component of atmospheric particulate matter (PM), sulfate at high concentrations will aggravate the formation of haze, thus causing serious air pollution and influencing human health (Sha et al., 2019; B. Zheng et al., 2015; Zhou et al., 2020). Moreover, sulfate is also one of the main species of acid deposition, reducing the pH values of rain droplets and aggravating acid rain (M. Liu et al., 2020; Lu, Fung, & Wu, 2015; K. Zheng et al., 2019). At the same time, sulfate is also the main

63 component of cloud condensation nuclei (CCN), which affects microphysical processes,
64 including the formation of clouds and precipitation, thus affecting solar radiation and climate
65 (Cziczo et al., 2013). Furthermore, sulfate itself is also one of the key short-lived species that has
66 negative radiative forcing (RF), which could influence the climate directly (Richardson et al.,
67 2019). Therefore, sulfate plays an essential role in the entire atmosphere and climate system.

68 　　In view of the fundamental roles of sulfate in many related fields, previous studies on
69 sulfate have made extensive, in-depth progress in recent decades. First, most regional
70 atmospheric monitoring studies have fully analyzed the appearance, source, temporal fluctuation
71 and spatial distribution of sulfate, as well as its proportion in PM. At the same time, modeling
72 studies have made great advances in revealing various mechanisms of SO_2 oxidation and sulfate
73 formation under different conditions and have greatly improved the performance of sulfate
74 simulation (Gao et al., 2016; G. Li et al., 2017; Luo, Yu, & Moch, 2020; Shao et al., 2019). For
75 instance, multiple studies emphasized the importance of aqueous-phase oxidation catalyzed by
76 transition metals in haze episodes (X. Huang et al., 2014; J. Li et al., 2020; Wang et al., 2021),
77 while other studies interpreted heterogeneous oxidation by NO_2 or HONO on the aerosol surface
78 as the dominant pathway, especially under conditions of high pH values and high NH_3
79 concentrations (Cheng et al., 2016; L. Huang et al., 2019; Yue et al., 2019; H. Zheng et al.,
80 2020). Some studies also analyzed the potential enhancement of sulfate formation by black
81 carbon (BC) (F. Zhang et al., 2020). In addition, wet deposition (WD) is the dominant removal
82 process for sulfate, accounting for more than 90% of its sink (Dentener et al., 2006; Driscoll,
83 Driscoll, Fakhraei, & Civerolo, 2016; B. Li et al., 2018; Qiao et al., 2015). Multiple studies have
84 discussed the simulation and observation of sulfate wet deposition in different regions and
85 periods, illustrating its great fluctuation and uncertainty in different models (Conradie et al.,
86 2016; Horowitz, 2006; Keene et al., 2015; Luo et al., 2020).

87 　　Furthermore, more studies have focused on RF and the climate response of sulfate. Some
88 of them discussed the sulfate RF both from anthropogenic sources and volcanic eruptions in the
89 upper troposphere and stratosphere (Aubry et al., 2021; C.-C. Chen & Gettelman, 2016; Flanner,
90 Gardner, Eckhardt, Stohl, & Perket, 2014; B. Li et al., 2018). Li et al. (2016) compared the
91 cooling effect of sulfate and warming effect of CO_2 and BC in China and concluded that the
92 negative RF of sulfate from intensive power and industry activities has offset most of the
93 warming factors. In contrast, studies have emphasized the weakened cooling effect or even
94 warming effect due to the rapid reduction in SO_2 emissions in China (Kasoar et al., 2016; M. Liu
95 & Matsui, 2021; X.-x. Ma, Liu, Wang, & Zhang, 2016). Moreover, sensitivity tests are often
96 used for sulfate to estimate its influence on global temperature and precipitation (e.g., increasing
97 the sulfate concentration to 5 or 10 times or removing anthropogenic SO_2 emissions) (Asutosh,
98 Fadnavis, Nuncio, Mueller, & Tripathy, 2021; Kasoar et al., 2016; L. Liu et al., 2018; Shawki,
99 Voulgarakis, Chakraborty, Kasoar, & Srinivasan, 2018).

100 　　However, all the studies mentioned above are still insufficient, especially in the
101 performance of sulfate simulation. First, although the surface monitoring networks in most
102 regions of the world have been gradually established and improved in recent years, the aircraft
103 measurement campaigns of sulfate are still relatively insufficient. For model studies, some of
104 them could only roughly reproduce the seasonal pattern of sulfate but had obvious biases in
105 simulating the magnitude of both near-surface concentrations and vertical distribution (Yang,
106 Wang, Smith, Easter, & Rasch, 2018). Although the chemical mechanisms have improved
107 remarkably, there are still significant overestimations of sulfate in different regions and seasons

in many regional and global models (Breider et al., 2017; Buchard et al., 2014; Georgiou et al., 2018; Lamarque et al., 2012; Lee et al., 2020; X. Li & Liu, 2013; X. Liu et al., 2012; Xiaohong Liu et al., 2007; Sobhani, Kulkarni, & Carmichael, 2018; Wei et al., 2019; Wu et al., 2020; Yang et al., 2018; B. Zhang et al., 2019). On the one hand, it may be related to the rapid reduction in SO_2 and sulfate emissions in many regions (especially in Europe, the United States (US) and China) during recent years, which has resulted in the sharp decline in the observed concentration of sulfate (de Meij et al., 2006; Fedkin, Li, Dickerson, Canty, & Krotkov, 2019; Syuichi Itahashi et al., 2018; H. Li et al., 2019; McClure & Jaffe, 2018; Sickles & Shadwick, 2015; Xie, Liu, Wang, & Wang, 2016). On the other hand, considering that the wet deposition of sulfate is derived from cloud formation and has great uncertainty (Breider et al., 2017; Z. Chen et al., 2019; Dentener et al., 2006; Echeverria, Abreu, Gonzalez, Ortega, & Echeverria, 2016; Horowitz, 2006; Luo et al., 2020), it also tends to be underestimated in some studies (S. Itahashi, 2018; Sedefian, Ku, Civerolo, Hao, & Zalewsky, 2016; Vivanco et al., 2017). An analysis of modeling studies suggests that the greatest uncertainty in global sulfur cycling is derived from the wet deposition of aerosol sulfate and the heterogeneous oxidation of SO_2 in clouds and aerosols (Faloona, 2009). As a result, the further evaluation of RF and the climate response of sulfate is likely to contain great uncertainty (Goto, Nakajima, Takemura, & Sudo, 2011; Ming, Ramaswamy, Ginoux, Horowitz, & Russell, 2005; Paulot, Paynter, Ginoux, Naik, & Horowitz, 2018; Stevens, 2015; Thornhill et al., 2021; Yang et al., 2017). Therefore, it is necessary to conduct further research on the simulation of sulfate concentration and RF and analyze the factors that lead to their uncertainties in detail.

This study aims to comprehensively evaluate and improve the performance of sulfate simulation in the Community Earth System Model 2 (CESM2), estimate the global RF of sulfate with the Parallel Offline Radiative Transfer (PORT) model, and, on this basis, discuss the factors influencing the simulation of sulfate concentration and RF. The descriptions of the CESM2 and PORT configuration as well as the observational data are introduced in section 2. The evaluation of sulfate simulations both near the ground and at high altitude will be shown in section 3. Next, the global RF of sulfate is estimated in section 4. Then, section 5 discusses the uncertainties associated with our simulations. Finally, key conclusions are presented in section 6.

2 Methodology

2.1 Model description

The simulations in this study are conducted with the Community Earth System Model 2 (CESM2 v2.1.3) (Danabasoglu et al., 2020; Louisa K. Emmons et al., 2020) and the Parallel Offline Radiative Transfer (PORT) model (Conley, Lamarque, Vitt, Collins, & Kiehl, 2013), both developed by the National Center for Atmospheric Research (NCAR, https://www.cesm.ucar.edu/models/cesm2/, last access: 13 June 2022). The CESM2 is a fully coupled global climate model configured with Community Atmosphere Model version 4.0 (CAM4) and coupled with the chemistry of Model for Ozone and Related chemical Tracers version 4 (MOZART-4) in this study (L. K. Emmons et al., 2010; Lamarque et al., 2012). Furthermore, we also incorporated a detailed in-cloud aqueous-phase chemistry module into MOZART-4 chemistry in the improved cases illustrated below, referring to the study of Ge et al. (2021).

150   The PORT model is a stand-alone radiative transfer model isolated with the CAM in the
151   CESM so that radiative fluxes can be computed without feedback on the surface. PORT can be
152   used for any radiation calculation. It implements stratospheric temperature adjustment under the
153   assumption of fixed dynamical heating, which is necessary for the computation of RF and
154   instantaneous radiative forcing (IRF) (Conley et al., 2013). Updated physics (CAM5) and a
155   radiation scheme (RRTMG) are used in this study.

156   Both models are configured with a horizontal resolution of 0.95° latitude and 1.25°
157   longitude and 30 levels from approximately 993 (near-surface layer) to 3.6 hPa in the vertical
158   direction. The offline meteorological data for model nudging are obtained from the Modern-Era
159   Retrospective analysis for Research and Applications version 2 (MERRA2,
160   https://rda.ucar.edu/datasets/ds313.3/, last access: 13 June 2022) (Gelaro et al., 2017; Molod,
161   Takacs, Suarez, & Bacmeister, 2015), all of whose temporal resolution is 3 h. All the emission
162   inventories needed for both models are obtained from the CESM database developed for CMIP6
163   projects   (https://svn-ccsm-
164   inputdata.cgd.ucar.edu/trunk/inputdata/atm/cam/chem/emis/emissions_ssp245/, last access: 13
165   June 2022) (L. Feng et al., 2020; Hoesly et al., 2018; McDuffie et al., 2020; Steven, Yuyu, &
166   Page, 2015). These inventories include both historical emissions from as early as 1750 to 2015
167   (annual) and predicted emissions from 2020 to 2100 (decade) under different climate scenarios
168   and are thus in accordance with the demands of the simulation periods in this study.

169   2.2 Model configuration

170   The basic information of all simulations conducted in this study is summarized in Table
171   S1. First, we conducted the simulation without any modification to the model (i.e., the Original
172   case). Then, the default parameterized SO_2 aqueous-phase reactions in the Original model were
173   replaced with detailed in-cloud aqueous-phase chemical mechanisms (Ge et al., 2021).
174   Furthermore, considering the high uncertainty of sulfate wet deposition parameterization in
175   models, a series of sensitivity simulations of sulfate wet deposition flux with different
176   adjustments (increased by factors of 5, 10, 15 and 20 (i.e., the Improved case)) were performed
177   to further optimize the simulation performance (Dentener et al., 2006; Horowitz, 2006).

178   On the basis of the Original and Improved simulations of CESM, the PORT model was
179   performed to determine the RF of sulfate. PORT is driven by model-generated datasets. In
180   addition to the datasets mentioned above, PORT also requires the sulfate concentrations
181   simulated by CESM cases as input files and then simulates and calculates the RF of sulfate
182   through the differences in its concentrations between different CESM cases. Therefore, we
183   further replaced the SO_2 emissions with their corresponding inventories in the preindustrial
184   period (1849-1850) and then simulated the global distributions of sulfate concentrations both in
185   the preindustrial period and without anthropogenic sources and their corresponding RFs with
186   PORT cases (Carslaw et al., 2017; Shawki et al., 2018; Smith et al., 2020; Thornhill et al., 2021).
187   Finally, in consideration of the factors that increase the uncertainty of sulfate RF simulation, a
188   series of sensitivity tests with the PORT model were conducted, which will be illustrated in
189   section 5 in detail.

190   Ultimately, all the simulations of this study run for a two-year period from 1 January
191   2014 to 31 December 2015, which is representative of the present day, or from 1 January 1849 to
192   31 December 1850, which is representative of the preindustrial era. The first year (2014 or 1849)
193   is used for model spin-up. The timestep used in both CESM and PORT is the default of 30

194   minutes. The output of the CESM simulation is the daily mean and is then converted to monthly
195   or seasonal means for analysis. The time interval of the input files of PORT is a default of 73
196   timesteps (i.e., 36.5 hours), and the output RF used in this study is in the form of a monthly mean
197   and is converted to an annual mean for analysis.

198   2.3 Surface monitoring networks and aircraft measurement campaigns

199   To better evaluate the performance of the model in simulating sulfate concentrations, the
200   observed data used in this study are collected from three surface monitoring networks and three
201   aircraft measurement campaigns. The locations of surface monitoring stations of different
202   networks and the flight regions and tracks of different aircraft campaigns are shown in Figure 1.
203   For surface observations, the data in Europe (EU) are obtained from the European Monitoring
204   and Evaluation Programme (EMEP, https://www.emep.int/, last access: 14 June 2022). The
205   observations in the US are obtained from the Interagency Monitoring of Protected Visual
206   Environments (IMPROVE, http://vista.cira.colostate.edu/Improve/, last access: 14 June 2022).
207   The observations in east and south Asia (EA and SA) are obtained from the Acid Deposition
208   Monitoring Network in East Asia (EANET, https://monitoring.eanet.asia/document/public/index,
209   last access: 14 June 2022). With regard to the aircraft observations, the Atmospheric
210   Tomography Mission data (ATom, https://daac.ornl.gov/cgi-bin/dsviewer.pl?ds_id=1925, last
211   access: 14 June 2022) are mostly measured over the ocean (Wofsy et al., 2021). The Wintertime
212   Investigation of Transport, Emission, and Reactivity observations (WINTER,
213   https://data.eol.ucar.edu/dataset/483.025, last access: 14 June 2022) are mainly carried out over
214   the sea and land of the eastern US (Green et al., 2019). The International Cooperative Air
215   Quality Field Study in Korea (KORUS-AQ, https://espo.nasa.gov/korus-aq/content/KORUS-AQ,
216   last access: 14 June 2022) is concentrated around South Korea (Lee et al., 2020).

217   All the surface observational data were directly collected from 1 January 2015 to 31
218   December 2015 in the form of daily averages and were further converted to monthly averages for
219   analysis. However, the aircraft measurements are relatively limited, and the observation year and
220   date may not match those of the simulation. Because the sulfate concentration in the same period
221   of adjacent years will not change significantly in terms of the order of magnitude, all the
222   simulated concentrations of sulfate were uniformly selected on the corresponding dates in 2015
223   for comparison. The flight dates of all aircraft measurements referred to in this study are listed in
224   Figures 3 and S2. For the convenience of comparison, the aircraft observed concentrations of
225   each flight were averaged by different altitude segments within the whole rectangular region as
226   defined in Figure 1. Then, the simulated concentrations were daily averages within the whole
227   rectangular flight region in each layer that covered the height range of the corresponding aircraft
228   measurements (J. Liu, Fan, Horowitz, & Levy, 2011). To make the comparison more
229   representative, these aircraft measurements cover different regions (as described above), altitudes
230   (approximately 2 km to 13 km) and months (March to August).

3 Improvements of global sulfate simulations

232   3.1 Differences in sulfate concentrations between the Original and Improved simulations

233   First, the seasonally averaged global distribution of the sulfate surface concentration
234   simulated in the Original case is shown in Figure 2, which exhibits significant spatial variability.
235   Most sulfate is concentrated in continental regions of the Northern Hemisphere, including

Europe (EU), North America (NAM), EA and SA, mainly from anthropogenic SO_2 emissions, such as energy and industrial activities), the Middle East (ME) and North Africa (NAF, mainly from natural sources). The sulfate concentrations in most of these regions exceed 5 $\mu g \cdot m^{-3}$ and even 20 $\mu g \cdot m^{-3}$ in some regions, especially in China and India, indicating pollution from intensive industrial activities. On the other hand, the sulfate concentrations are relatively low over oceans and generally less than 5 $\mu g \cdot m^{-3}$ in most regions, mainly from the oxidation of DMS.
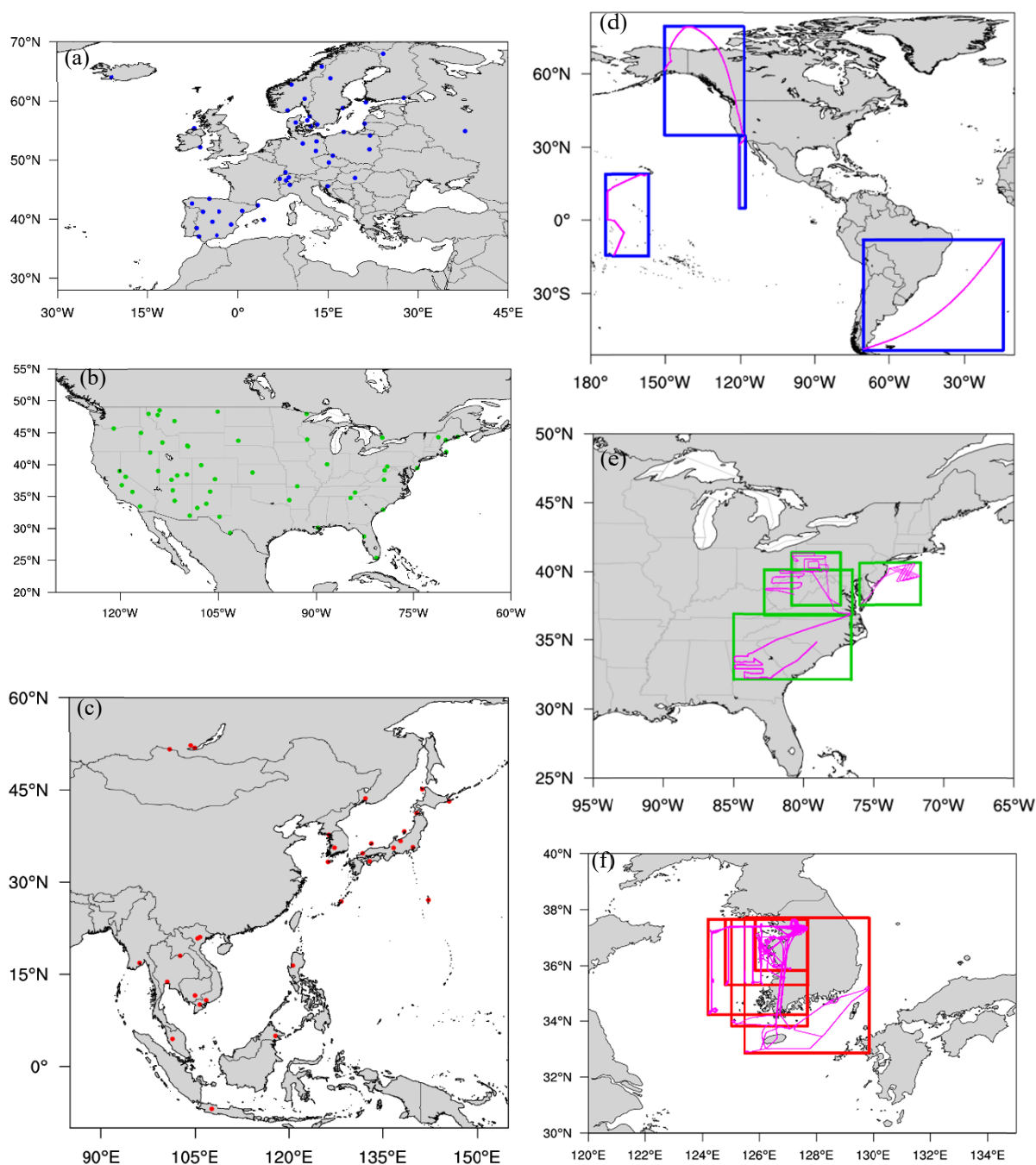
Figure 1. Locations of monitoring sites from three surface measurement networks in (a) EU (EMEP), (b) US (EPA) and (c) EA and flight ranges of three aircraft measurement campaigns, including (d) ATom, (e) WINTER and (f) KORUS-AQ, at different times. The pink lines are the tracks of each flight.

In terms of seasons, however, there is no significant and consistent distributional characteristic worldwide. In general, the concentrations in both hemispheres are slightly higher in spring and summer than in autumn and winter but do not fluctuate intensively in different seasons, which is obviously different from that of SO_2 (Ge et al., 2021). Such differences are related to the combination of precursor emissions and atmospheric oxidation capacity. In summer, the sulfur emissions are relatively weak due to the decreased demand for heating. Sufficient sunlight and high temperature in summer enhance the oxidation capacity at the same time, which promotes the formation of ·OH radicals and sulfate. These simulations are the opposite in winter.

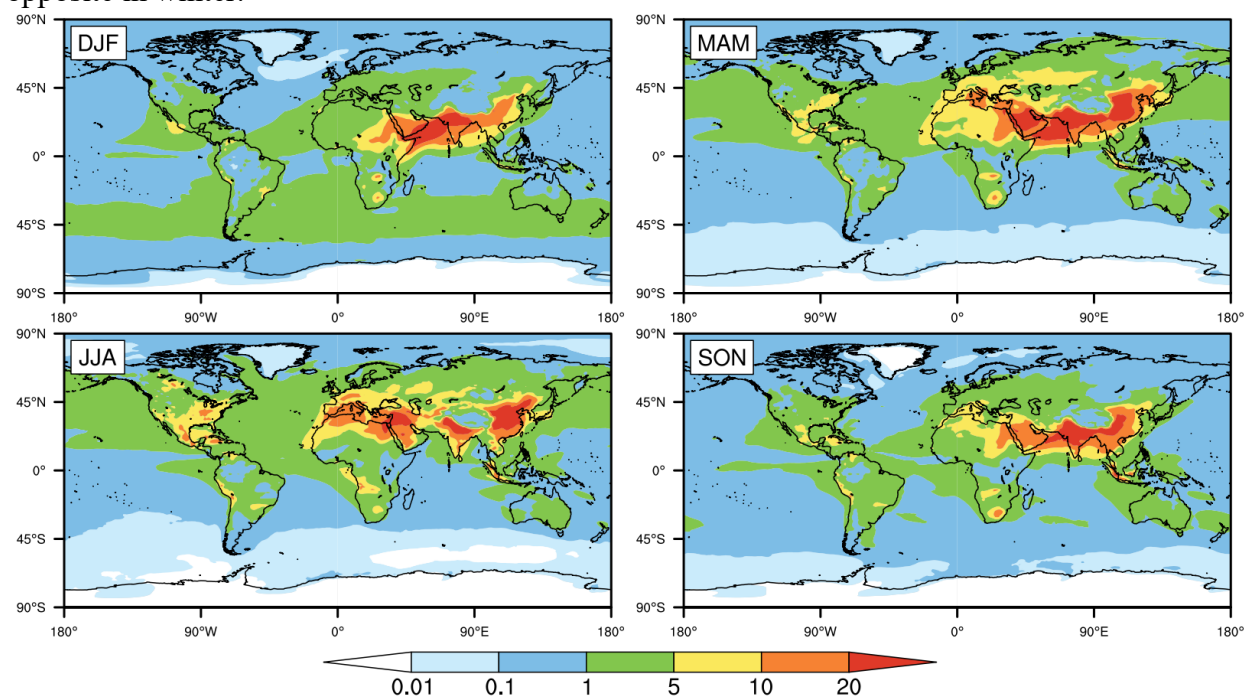**Figure 2. Global distribution of seasonally averaged surface concentrations of sulfate (unit: $\mu g \cdot m^{-3}$) in 2015, simulated by CESM2 with standard configuration (i.e., the Original case). DJF, MAM, JJA and SON represent December-January-February, March-April-May, June-July-August and September-October-November, respectively, which is the same below.**

262   After incorporating the detailed in-cloud aqueous-phase chemical mechanisms and
263 enhancing the WD rate of sulfate, the concentrations of sulfate dropped markedly in all seasons,
264 as shown in Figure 3. In general, the reductions in sulfate do not exceed 5 μg·m^{-3} in most
265 regions, especially over the ocean. In some regions, such as EA, SA and ME, the sulfate
266 concentrations can still decrease by more than 10 μg·m^{-3}. This distribution is high, corresponding
267 to that of the simulated background sulfate concentrations shown in Figure 2. Similarly, there are
268 no distinct seasonal differences in sulfate reduction. The reduction in spring and summer is only
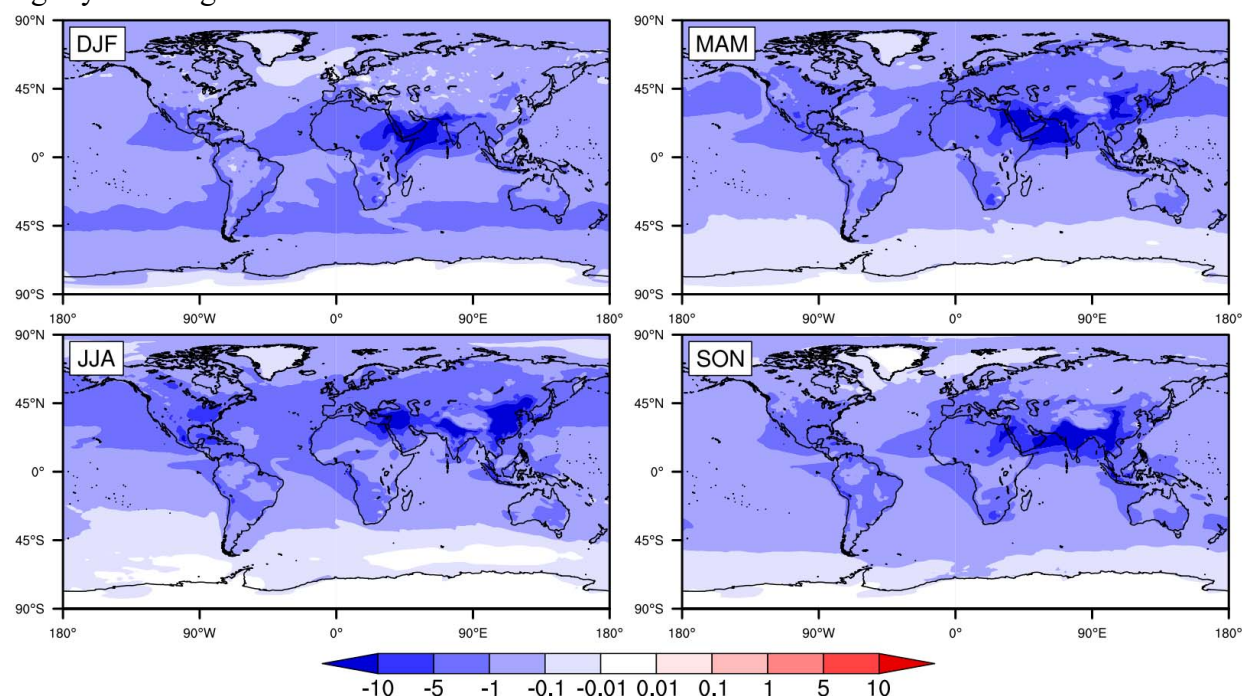269 slightly more significant than that in autumn and winter.

270
271 **Figure 3. The differences in global seasonally averaged surface sulfate concentrations (unit:**

272 **μg·m^{-3}) between the Improved case and the Original case in 2015 after incorporation of**

273 **detailed in-cloud aqueous-phase chemical mechanisms and enhanced wet deposition flux of**

274 **sulfate (i.e., Case 6 minus Case 1).**

275   3.2 Comparison between the simulated and observed surface sulfate concentrations

276   A comparison with the observations of sulfate in different regions exhibits the accuracy
277 of the model simulation of sulfate. Figure 4 shows the observed and simulated monthly average
278 surface sulfate concentrations in the three monitoring networks over the EU (EMEP), NAM
279 (IMPROVE) and Asia (EANET). The observations from the EANET monitoring network are
280 further divided into "Japan and South Korea" and "Other Asia countries", as shown in Figure S1.
281 First, the observed concentrations of sulfate in all three regions mentioned above are relatively
282 consistent throughout the year without large fluctuations. Compared with the observations, it is
283 noteworthy that the surface sulfate concentrations in the Original simulation are severely
284 overestimated in all three regions and in almost all months, especially from April to September.

285 The coupling of detailed in-cloud aqueous-phase
286 chemical mechanisms enhances the oxidation
287 capacity of SO_2 and further increases the sulfate
288 concentration, especially in autumn and winter in
289 EU and NAM and throughout the year in AS. As
290 indicated in Ge et al. (2021), the coupling of
291 detailed in-cloud chemistry significantly lowers SO_2
292 concentrations and fits well with the observations.
293 However, this results in a larger overestimation of
294 sulfate. After adjusting the WD flux of sulfate, the
295 concentrations decreased considerably in nearly all
296 months. The greater the WD flux is, the lower the
297 sulfate concentration is. Notably, the sulfate
298 concentrations drop the most significantly at 5 times
299 the Original WD flux and show a small, further
300 decrease when switching to 10 or 20 times the
301 Original WD flux. Regardless of the region, the
302 simulations show remarkable improvement, and
303 nearly all the Improved surface sulfate
304 concentrations are within the range of the standard
305 deviation of the observations, with the exception of
306 summer in the EU. The notable overestimates in the
307 EU in July and August may be related to the
308 Mediterranean climate with insufficient
309 precipitation in summer in parts of the EU, leading
310 to the limited effect of sulfate WD.

311 **Figure 4. Monthly average surface sulfate**

312 **concentrations (μg·m^{-3}) in EU, NAM, and Asia in**

313 **2015. The black solid lines and red dashed lines**

314 **represent the observed and Original simulated**

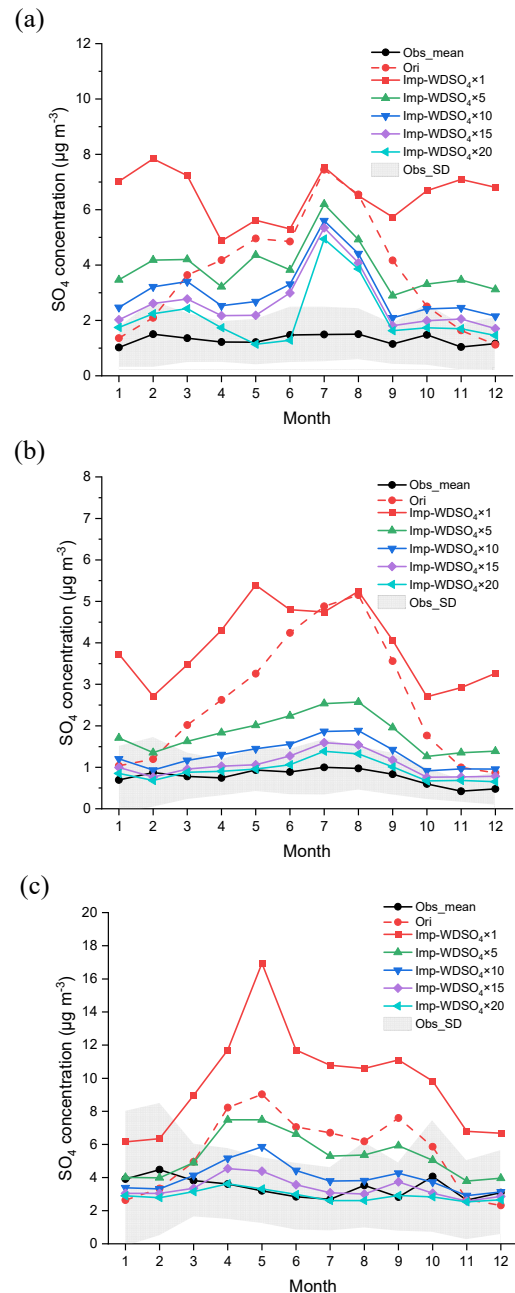315 **concentrations, respectively. Other lines**

316 **represent improved sulfate concentrations with**

317 **different levels of sulfate wet deposition fluxes. The multiples of sulfate wet deposition from**

318 **top to bottom are 1, 5, 10, 15 and 20 (i.e., the Improved case). The gray areas represent the**

319 **standard deviation of the observed concentrations. The observed concentrations are**

320 **calculated by averaging the data from all monitoring stations over a region. The simulated**

321 **concentrations are calculated by averaging the data from all the grids where the**

322 **monitoring stations are located. The corresponding monitoring networks are (a) EMEP, (b)**

323 **IMPROVE and (c) EANET.**

324 3.3 Comparison between the simulated and aircraft observations

325 In addition to surface concentrations, sulfates at higher altitudes are also very important
326 in terms of their climate effects on clouds and radiation and are thus compared with various
327 aircraft measurements (see Figures 5 and S2). First, regardless of the aircraft measurement or
328 simulation case, the distribution of sulfate concentration changes substantially with height (from
329 more than 10 $\mu g \cdot m^{-3}$ near the surface to near 0 $\mu g \cdot m^{-3}$ at higher altitudes). Overall, the sulfate is
330 concentrated near the ground and decreases with increasing height. Similar to the results of the
331 surface sulfate concentration, when compared with the aircraft observations, the results of the
332 Original case are notably overestimated, especially at low altitudes and near the ground. The
333 coupling of in-cloud aqueous-phase mechanisms still further increases the sulfate concentration
334 to some extent. After enhancing the WD flux, sulfate concentrations decrease markedly. The
335 declining characteristics with different multiples are basically consistent with the surface sulfate
336 results. That is, the higher the multiple is, the lower the concentration is and the smaller the
337 decrease range is. Finally, most of the Improved sulfate concentrations at different altitudes are
338 within the range of the standard deviation of aircraft observations. The overestimation of sulfate
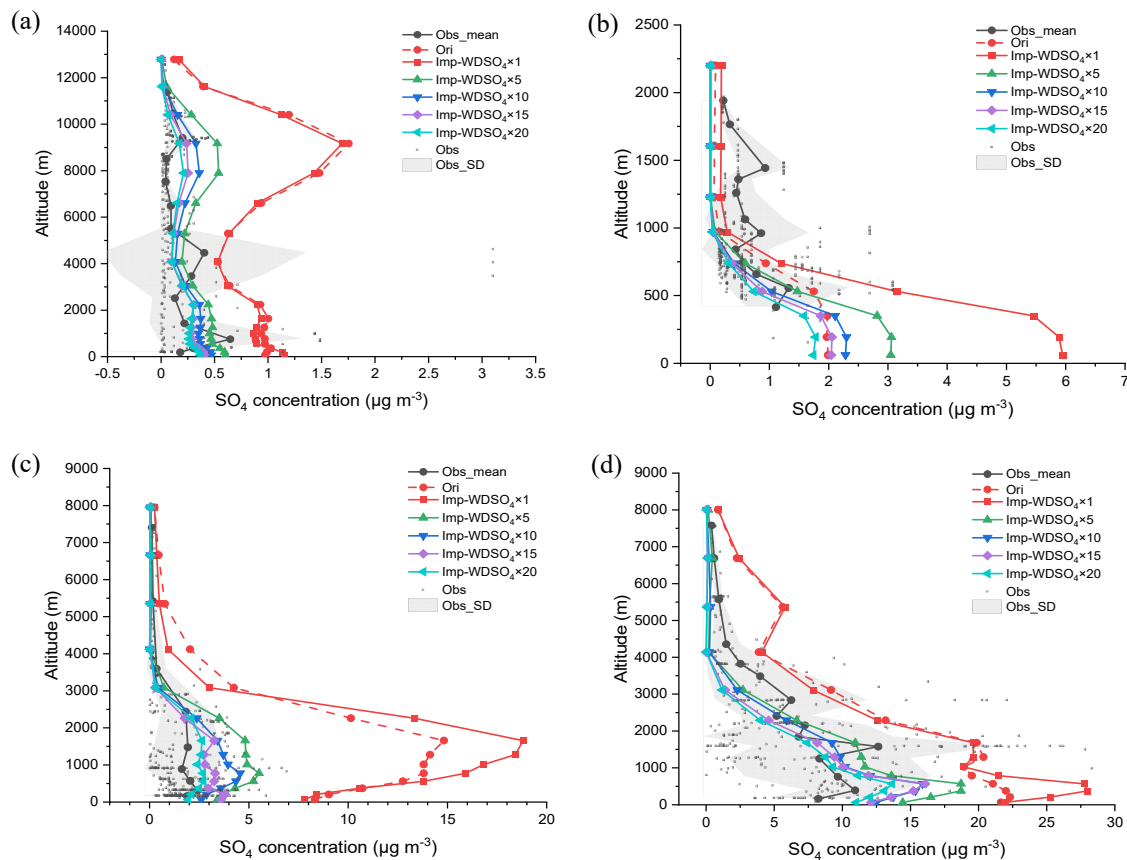339 concentrations at low altitudes has been greatly mitigated.
340

Figure 5. Vertical profiles of sulfate concentrations (μg·m⁻³) over different regions. The black solid lines represent the average observed concentrations at different altitudes. The red dashed lines represent the Original simulated concentrations on the same day in 2015. Other lines represent improved sulfate concentrations with different levels of sulfate wet deposition fluxes. The multiples of sulfate wet deposition from top to bottom are 1, 5, 10, 15 and 20 (i.e., the Improved case). The gray areas represent the standard deviation of the observed concentrations. The black dots represent every single observational data point. The corresponding aircraft measurement campaigns are (a) ATom on 15 August 2016, (b) WINTER on 3 March 2015 and (c-d) KORUS-AQ on 10 May 2016 and 30 May 2016.

Nevertheless, the sulfate concentrations at high altitudes are underestimated in some cases. Therefore, lines of the observed and simulated results generally meet at the boundary layer height (overestimate at lower levels and underestimate at higher levels), ranging from 1 to 4 km, as shown in Figures 5 and S2 (Kipling et al., 2016). All the deviations in the sulfate concentration simulation at different altitudes and the variability in cross regions may lead to great uncertainty in the subsequent assessment of the RF of sulfate. Therefore, we performed a series of sensitivity tests on RF in section 5.

In summary, the incorporation of in-cloud aqueous-phase mechanisms and an increase in sulfate WD greatly decreases the concentration and mitigates the deviation in the sulfate simulation, thus significantly improving the overall performance of sulfate simulation both near the ground and at high altitudes.

4 Global radiative forcing from the sulfate distribution

4.1 Radiative forcing of sulfate in different sensitivity simulations

Sulfate has a cooling effect on climate. Therefore, the substantial reduction in simulated sulfate concentrations after improvement will elevate its RF (Figure 6). Clearly, the RF of sulfate increases evidently in all seasons and nearly all regions worldwide, which means an improved global sulfate distribution may weaken its cooling effect significantly. Similar to the results in Figures 2 and 3, such an increase in RF is also distributed unevenly throughout the world, mainly in EA, SA, ME, EU and in low- and middle-latitude regions, where the value usually exceeds 5 W·m⁻². Most high-latitude regions are rarely affected, and the increase is no more than 0.5 W·m⁻², which is in accordance with the relatively low background distribution of the sulfate concentration. Although the increase is greater in spring and summer to some extent, the fluctuation is not intense throughout the year. Overall, the incorporation of in-cloud aqueous-

373 phase mechanisms and an increase in sulfate WD lead to lower SO_2/sulfate concentrations and a
374 smaller cooling effect of sulfate, as shown in Figures 7 and S3.

375   4.2 Radiative forcing of global anthropogenic sulfate

376   The incorporation of in-cloud aqueous-phase mechanisms and an increase in sulfate WD
377 could affect the simulation of sulfate RF from anthropogenic emissions since 1750. The RF of
378 sulfate in 2011 relative to 1750 (-0.41 W·m^{-2}, -0.62 to -0.21 W·m^{-2}) was provided in the fifth
379 report of IPCC (Intergovernmental Panel on Climate, 2014), as shown in Figure 7. We also
380 referred to and summarized several previous studies related to the assessment of sulfate RF in
381 Figure 7. Moreover, the results of our Original and Improved simulations of sulfate RF in 2015
382 relative to 1850 are also shown in Figures 7 and S3. We also simulated the corresponding two
383 RFs of all anthropogenic sulfates by complete removal of all anthropogenic emissions (i.e.,
384 Original and Improved anthro-removed simulations). Compared with the results of the IPCC
385 report, it is obvious that the RF of sulfate in the Original simulations is severely overestimated.
386 The incorporation of in-cloud aqueous-phase mechanisms and an increase in sulfate WD
387 markedly reduce the overestimation. The corresponding two improved-simulated RFs are -0.382
388 and -0.410 W·m^{-2}, which are comparable to the IPCC report and other, previous studies (Chuang,
389 Penner, Taylor, Grossman, & Walton, 1997; Haywood & Ramaswamy, 1998; B. Li et al., 2018;
390 X. Ma, Shi, Guo, & Wang, 2005; Matus, L'Ecuyer, & Henderson, 2019; Ni, Zheng, Ma, Wang,
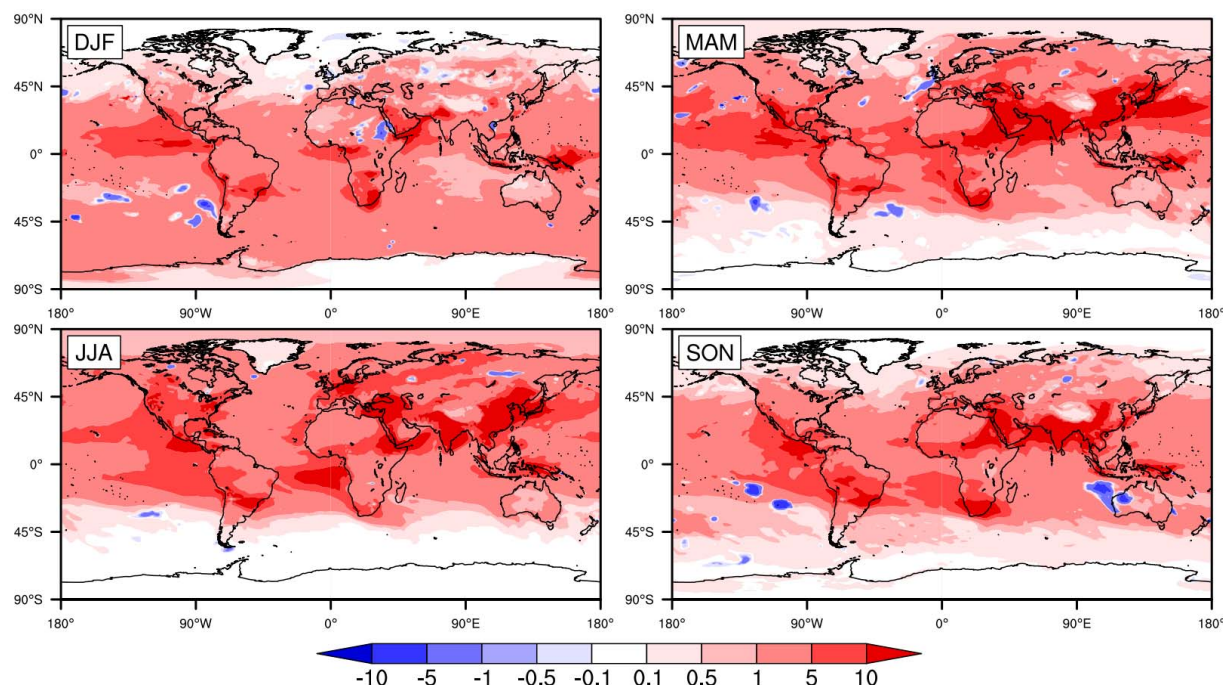391 & Wang, 2016; Penner, Chuang, & Grant, 1998).
392

393 **Figure 6. The differences in global seasonally averaged sulfate radiative forcing (unit:**

394 **W·m^{-2}) between the Improved case and the Original case in 2015 after the incorporation of**

395   **detailed in-cloud aqueous-phase chemical mechanisms and multiplication of the wet**

396   **deposition flux of sulfate.**

397   The results indicate that the current model tends to overestimate the sulfate concentration,
398   which in turn leads to overestimation of the negative RF and cooling effect of sulfate. After the
399   incorporation of in-cloud aqueous-phase mechanisms and enhancement of sulfate WD, the
400   simulations could significantly mitigate the deviation in the concentration and RF assessments of
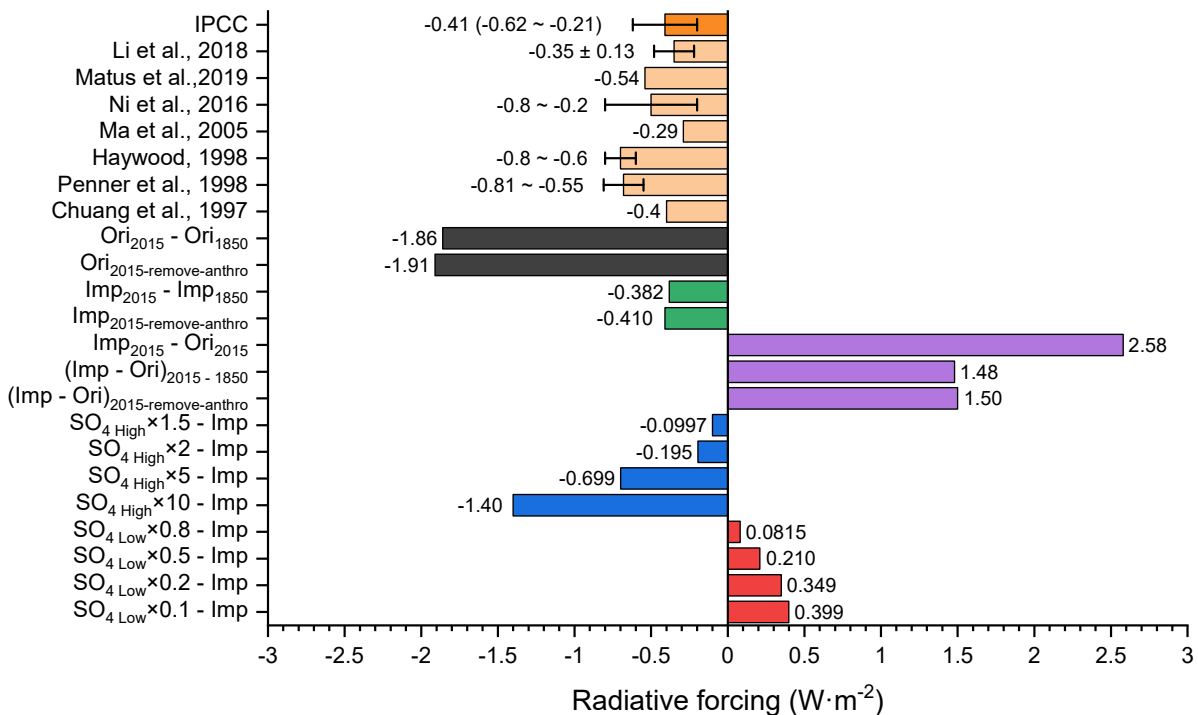401   sulfate. Such improvements could also verify the reliability of the IPCC report.

402
403   **Figure 7. Radiative forcing of sulfate in different simulation cases and references (Chuang**

404   **et al., 1997; Haywood & Ramaswamy, 1998; Intergovernmental Panel on Climate, 2014; B.**

405   **Li et al., 2018; X. Ma et al., 2005; Matus et al., 2019; Ni et al., 2016; Penner et al., 1998).**

406   **5 Factors influencing the simulation of sulfate radiative forcing and uncertainty analysis**

407   Model evaluation shows an underestimation of sulfate concentration at high altitudes but
408   overestimation within the boundary layer (shown in sections 3.2 and 3.3). This finding would
409   lead to great uncertainty in the estimate of sulfate RF. To understand the potential variability in
410   sulfate RF, we conducted additional sensitivity tests, as shown in Figure 8. To better fit the
411   simulated sulfate concentration with the aircraft observations, we enhance sulfate concentrations
412   by factors of 1~10 above the boundary layer and reduce boundary layer sulfate concentrations by
413   factors of 1~0.1. The demarcation height of these two uncertainty factors is set to 2.0 km, and

414   four additional levels (1.2, 1.5, 2.7, and 3.6 km) were also added given the range of this value
415   from 1 to 4 km in section 3.3.

416   Figure 8 shows the differences in sulfate RF between all the sensitivity tests and the
417   Improved case. The corresponding global annual distributions are shown in Figures S4-5. The
418   RF values in Figure 8a increase from left to right, indicating that the decrease in sulfate
419   concentration at low altitude leads to weakening of the cooling effect of sulfate and increases the
420   RF values from the Improved case. The maximum difference value is +0.399 W·m^{-2} when the
421   sulfate concentration below 2.0 km is reduced by 90%, as shown in Figure 7. On the other hand,
422   the values decrease from bottom to top, indicating that the increase in sulfate concentration at
423   high altitudes strengthens the cooling effect of sulfate and results in negative RF values.
424   Similarly, when the sulfate concentration above 2.0 km increases by a factor of 10, the RF value
425   is reduced by 1.40 W·m^{-2} from the Improved case.

426

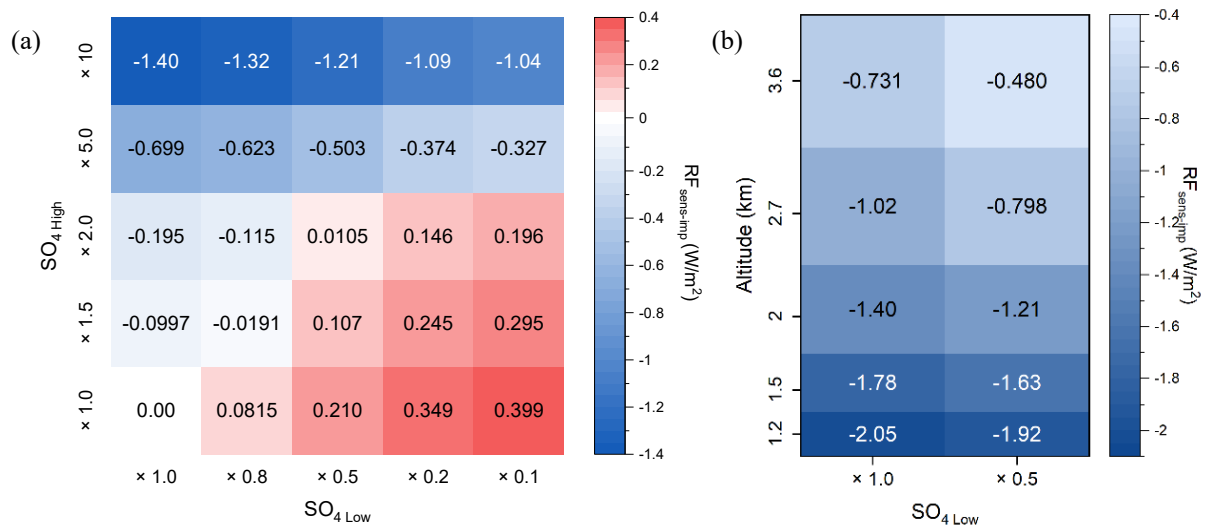427   **Figure 8. The differences in annual global-mean sulfate radiative forcing (unit: W·m^{-2})**

428   **between each sensitivity test and the Improved case in 2015. (a) The horizontal direction is**

429   **the sensitivity test for decreasing the sulfate concentration at low altitude (below 2.0 km).**

430   **The decrease factors from left to right are 1.0, 0.8, 0.5, 0.2, and 0.1, indicating that the**

431   **sulfate concentrations below 2.0 km are 100%, 80%, 50%, 20% and 10% of the Improved**

432   **case, respectively. The vertical direction is the sensitivity test for increasing the sulfate**

433   **concentration at high altitudes (above 2.0 km). The increase factors from bottom to top are**

434   **1.0, 1.5, 2.0, 5.0, and 10. (b) The vertical direction is the sensitivity test of changing the**

435   **altitude of the turning point (TP, the altitude above which the model tends to**

436 **underestimate sulfate concentrations and below which the model tends to overestimate**

437 **sulfate concentrations). The altitudes of the TP are set from bottom to top as 1.2, 1.5, 2.0,**

438 **2.7, and 3.6 km. The decreasing factors for sulfate concentration at low altitude are 1.0 and**

439 **0.5, and the increasing factor for sulfate concentration at high altitude is 10.**

440   Notably, the sulfate RF basically shows a linear trend with its concentration. At the same
441 time, the differences between the bundles "1.0×1.0" (0 $W \cdot m^{-2}$) and "2.0×1.0" (-0.195 $W \cdot m^{-2}$) is -
442 0.195 $W \cdot m^{-2}$, indicating that the RF was contributed by sulfate above 2.0 km. Then, according to
443 the maximum (+0.399 $W \cdot m^{-2}$) above, we can roughly estimate that the ratio of sulfate content
444 between "< 2.0 km" and ">2.0 km" is 2.2:1, which means that most sulfate is concentrated near
445 the ground. In addition, from the two RFs above, we can generally determine that the total RF of
446 sulfate, including anthropogenic and natural sources, is 0.63 $W \cdot m^{-2}$. Then, compared with the RF
447 of anthropogenic sulfate only (-0.410 $W \cdot m^{-2}$) shown in Figure 7, we could also roughly estimate
448 that the RF of natural sulfate is approximately -0.22 $W \cdot m^{-2}$, and the ratio between anthropogenic
449 and natural sulfate RF is approximately 1.8:1, which means that natural sources from the ocean
450 (e.g., DMS) contribute approximately one-third of sulfate RF, and anthropogenic emissions
451 account for the remaining two-thirds.

452   In conclusion, the overestimation of the sulfate concentration near the ground would in
453 turn overestimate its cooling effect to some extent. The removal of excess sulfate would lessen
454 the negative RF of sulfate. In contrast, the underestimation of sulfate at high altitudes would
455 further lead to the underestimation of sulfate RF. The supplement for such underestimation will
456 significantly increase the negative RF of sulfate, which indicates that the underestimated sulfate
457 at high altitudes in the simulation has a much stronger cooling potential. Therefore, the
458 overestimation or underestimation of sulfate concentrations at different heights will significantly
459 increase the deviation and uncertainty of the evaluation of sulfate RF.

460   Finally, with regard to the sensitivity tests of changing the TP altitude, Figure 8b shows
461 that whether the decrease factors at low altitude are 1.0 or 0.5, the negative sulfate RF increases
462 with the decrease in TP. The downward movement of the TP enlarges the high-altitude area
463 where the model underestimates sulfate concentrations and therefore increases the negative RF
464 of sulfate. When the TP drops to 1.2 km, the sulfate RF can be further decreased by up to 2.05
465 $W \cdot m^{-2}$ based on the Improved-simulation. The opposite is true when elevating the TP altitude,
466 which expands the low-altitude area and weakens the cooling effect of sulfate. Furthermore, it
467 should be noted that various aircraft observations in section 3.3 involve different time periods
468 throughout the year and different regions around the world. This understanding infers a much
469 broader fluctuation of the TP altitudes when comparing the simulated and observed sulfate
470 concentrations at annual and global scales, which might also bring substantial uncertainties to the
471 evaluation of sulfate RF.

472   Based on the analysis above, although the improved RF of sulfate estimated in this study
473 is close to that of the IPCC report, there is the potential that the true sulfate RF may deviate
474 significantly from either this study or the IPCC report. This deviation may partly come from the

475 uncertainty of emission inventories, sulfur chemistry and sulfate wet deposition during model
476 simulations. Therefore, it is necessary to update relevant emission data in a timely manner and
477 strengthen the field study of sulfate in terms of its concentrations and wet deposition at different
478 altitudes and regions and seasons to mitigate the uncertainty of sulfate RF and provide a more
479 reliable assessment of climate change.

480 **6 Conclusions and discussion**

481   In view of the uncertainty of global simulation of sulfate concentration and the related
482 RF, this study used CESM2 and PORT models to evaluate and improve their simulation
483 performance of sulfate. After the incorporation of detailed in-cloud aqueous-phase chemical
484 mechanisms and enhanced wet deposition flux of sulfate, the simulation of sulfate concentration
485 improved significantly both near the ground and at high altitude compared with observations.
486 Consequently, such improvement in simulations of sulfate distribution further improved the
487 simulation of sulfate RF. The Improved-simulated RFs of sulfate from 1850 to 2015 and all
488 anthropogenic sources are -0.382 and -0.410 $W \cdot m^{-2}$, respectively, which are both comparable to
489 the IPCC report and other, previous studies. Our results indicated that the wet deposition of
490 sulfate is one of the important sources of uncertainty in its concentration simulation.
491 Furthermore, the surface overestimation and high-altitude underestimation of sulfate are the main
492 uncertainty factors of the sulfate RF simulation. As reported in IPCC AR5 and 6, aerosols
493 partially offset the RF of well-mixed greenhouse gases, which is the most uncertain part of the
494 total anthropogenic forcing in climate change (Intergovernmental Panel on Climate, 2014; B. Li
495 et al., 2018; H. Zhang & Huang, 2014). As an important component of aerosols and sources of
496 negative forcing, sulfate, with its wet scavenging and related cloud processes, remains a key
497 source of uncertainty in the estimation of global RF.

498   Many countries and regions (e.g., EU, US, Japan and China) have focused more attention
499 and efforts on air pollution control in recent years, and the emissions and concentrations of PM
500 and sulfate in the atmosphere have decreased rapidly (Aas et al., 2019; Attwood et al., 2014;
501 Breider et al., 2017; Dai et al., 2021; J. Feng et al., 2021; Karplus, Zhang, & Almond, 2018;
502 Rogora, Colombo, Marchetto, Mosello, & Steingruber, 2016; Yan & Xu, 2021). Therefore, the
503 emission data sources need to be updated promptly. Moreover, it is worth emphasizing that since
504 the lifetime of sulfate is relatively short compared with that of CO_2, the climate response from
505 sulfate emission changes may happen at a much faster pace than CO_2. If global models
506 underestimate the sulfate cooling effects at high altitudes, they could already counteract the
507 warming effect of CO_2 significantly. As an increasing number of countries set carbon neutral
508 targets for the near future and rapidly phase out the use of fossil energy, anthropogenic sulfur
509 emissions will decline accordingly, which may cause a much more intensive warming effect than
510 expected in the short term, especially in China. Notably, various policies aiming to reduce
511 pollution over China have resulted in a dramatic decrease in aerosols, causing in an overall
512 warming effect due to the dominant role of sulfate reductions in the period of 2012~2021 (Bae,
513 Kim, Kim, Kim, & Kim, 2021; Fioletov et al., 2016; Geng et al., 2019; Jo et al., 2020; X. Li et
514 al., 2020). "Carbon peaking" and "carbon neutrality" goals were first announced in 2020 in
515 China. Consequently, the energy and industrial structures of these regions are bound to transform
516 gradually in the future, followed by remarkable changes in the emissions and levels of various
517 pollutants, including sulfate. Therefore, it is of great importance to estimate the RF of short-lived

518 pollutants and its contribution to global climate change in the following decades. All these issues
519 will be examined in our future work.

Acknowledgments

Open Research

525 The Community Earth System Model 2 (CESM2) developed by the National Center for Atmospheric
526 Research can be downloaded online (https://www.cesm.ucar.edu/models/cesm2/). All codes used to
527 generate the results of this study are available from the authors upon request. The CMIP6 emission
528 datasets analyzed during the current study are available at https://svn-ccsm-
529 inputdata.cgd.ucar.edu/trunk/inputdata/atm/cam/chem/. The MERRA2 meteorological offline data
530 are publicly available from https://rda.ucar.edu/datasets/ds313.3/.

531

532

References

534 Aas, W., Mortier, A., Bowersox, V., Cherian, R., Faluvegi, G., Fagerli, H., . . . Xu, X. (2019).
535 Global and regional trends of atmospheric sulfur. *Scientific Reports, 9*. doi:10.1038/s41598-018-
536 37304-0

537 Asutosh, A., Fadnavis, S., Nuncio, M., Mueller, R., & Tripathy, S. C. (2021). The Arctic
538 Temperature Response to Global and Regional Anthropogenic Sulfate Aerosols. *Frontiers in
539 Environmental Science, 9*. doi:10.3389/fenvs.2021.766538

540 Attwood, A. R., Washenfelder, R. A., Brock, C. A., Hu, W., Baumann, K., Campuzano-Jost, P., .
541 . . Brown, S. S. (2014). Trends in sulfate and organic aerosol mass in the Southeast U.S.: Impact

542   on aerosol optical depth and radiative forcing. *Geophysical Research Letters, 41*(21), 7701-7709.

543   doi:10.1002/2014gl061669

544   Aubry, T. J., Staunton-Sykes, J., Marshall, L. R., Haywood, J., Abraham, N. L., & Schmidt, A.

545   (2021). Climate change modulates the stratospheric volcanic sulfate aerosol lifecycle and

546   radiative forcing from tropical eruptions. *Nature Communications, 12*(1). doi:10.1038/s41467-

547   021-24943-7

548   Bae, M., Kim, B.-U., Kim, H. C., Kim, J., & Kim, S. (2021). Role of emissions and meteorology

549   in the recent $PM_{2.5}$ changes in China and South Korea from 2015 to 2018. *Environmental*

550   *Pollution, 270*. doi:10.1016/j.envpol.2020.116233

551   Breider, T. J., Mickley, L. J., Jacob, D. J., Ge, C., Wang, J., Sulprizio, M. P., . . . Hopke, P. K.

552   (2017). Multidecadal trends in aerosol radiative forcing over the Arctic: Contribution of changes

553   in anthropogenic aerosol to Arctic warming since 1980. *Journal of Geophysical Research-*

554   *Atmospheres, 122*(6), 3573-3594. doi:10.1002/2016jd025321

555   Buchard, V., da Silva, A. M., Colarco, P., Krotkov, N., Dickerson, R. R., Stehr, J. W., . . . He, H.

556   (2014). Evaluation of GEOS-5 sulfur dioxide simulations during the Frostburg, MD 2010 field

557   campaign. *Atmospheric Chemistry and Physics, 14*(4), 1929-1941. doi:10.5194/acp-14-1929-

558   2014

559   Carslaw, K. S., Gordon, H., Hamilton, D. S., Johnson, J. S., Regayre, L. A., Yoshioka, M., &

560   Pringle, K. J. (2017). Aerosols in the Pre-industrial Atmosphere. *Current Climate Change*

561   *Reports, 3*(1), 1-15. doi:10.1007/s40641-017-0061-2

562   Chen, C.-C., & Gettelman, A. (2016). Simulated 2050 aviation radiative forcing from contrails

563   and aerosols. *Atmospheric Chemistry and Physics, 16*(11), 7317-7333. doi:10.5194/acp-16-7317-

564   2016

565 Chen, Z., Huang, T., Huang, X., Han, X., Yang, H., Cai, Z., . . . Huang, C. (2019).

566 Characteristics, sources and environmental implications of atmospheric wet nitrogen and sulfur

567 deposition in Yangtze River Delta. *Atmospheric Environment, 219*.

568 doi:10.1016/j.atmosenv.2019.116904

569 Cheng, Y., Zheng, G., Wei, C., Mu, Q., Zheng, B., Wang, Z., . . . Su, H. (2016). Reactive

570 nitrogen chemistry in aerosol water as a source of sulfate during haze events in China. *Science*

571 *Advances, 2*(12). doi:10.1126/sciadv.1601530

572 Chuang, C. C., Penner, J. E., Taylor, K. E., Grossman, A. S., & Walton, J. J. (1997). An

573 assessment of the radiative effects of anthropogenic sulfate. *Journal of Geophysical Research-*

574 *Atmospheres, 102*(D3), 3761-3778. doi:10.1029/96jd03087

575 Conley, A. J., Lamarque, J. F., Vitt, F., Collins, W. D., & Kiehl, J. (2013). PORT, a CESM tool

576 for the diagnosis of radiative forcing. *Geoscientific Model Development, 6*(2), 469-476.

577 doi:10.5194/gmd-6-469-2013

578 Conradie, E. H., Van Zyl, P. G., Pienaar, J. J., Beukes, J. P., Galy-Lacaux, C., Venter, A. D., &

579 Mkhatshwa, G. V. (2016). The chemical composition and fluxes of atmospheric wet deposition

580 at four sites in South Africa. *Atmospheric Environment, 146*, 113-131.

581 doi:10.1016/j.atmosenv.2016.07.033

582 Cziczo, D. J., Froyd, K. D., Hoose, C., Jensen, E. J., Diao, M., Zondlo, M. A., . . . Murphy, D.

583 M. (2013). Clarifying the Dominant Sources and Mechanisms of Cirrus Cloud Formation.

584 *Science, 340*(6138), 1320-1324. doi:10.1126/science.1234145

585 Dai, T., Cheng, Y., Goto, D., Li, Y., Tang, X., Shi, G., & Nakajima, T. (2021). Revealing the

586 sulfur dioxide emission reductions in China by assimilating surface observations in WRF-Chem.

587 *Atmospheric Chemistry and Physics, 21*(6), 4357-4379. doi:10.5194/acp-21-4357-2021

588   Danabasoglu, G., Lamarque, J. F., Bacmeister, J., Bailey, D. A., DuVivier, A. K., Edwards, J., . .

589   . Strand, W. G. (2020). The Community Earth System Model Version 2 (CESM2). *Journal of*

590   *Advances in Modeling Earth Systems, 12*(2), 1-35. doi:10.1029/2019ms001916

591   de Meij, A., Krol, M., Dentener, F., Vignati, E., Cuvelier, C., & Thunis, P. (2006). The

592   sensitivity of aerosol in Europe to two different emission inventories and temporal distribution of

593   emissions. *Atmospheric Chemistry and Physics, 6*, 4287-4309. doi:10.5194/acp-6-4287-2006

594   Dentener, F., Drevet, J., Lamarque, J. F., Bey, I., Eickhout, B., Fiore, A. M., . . . Wild, O. (2006).

595   Nitrogen and sulfur deposition on regional and global scales: A multimodel evaluation. *Global*

596   *Biogeochemical Cycles, 20*(4). doi:10.1029/2005gb002672

597   Driscoll, C. T., Driscoll, K. M., Fakhraei, H., & Civerolo, K. (2016). Long-term temporal trends

598   and spatial patterns in the acid-base chemistry of lakes in the Adirondack region of New York in

599   response to decreases in acidic deposition. *Atmospheric Environment, 146*, 5-14.

600   doi:10.1016/j.atmosenv.2016.08.034

601   Echeverria, M., Abreu, C. M., Gonzalez, A., Ortega, A., & Echeverria, C. A. (2016). Towards

602   the Determination of the Origin of Sulfur Compounds in Marine Zones by Means of the

603   Chloride/Sulfate Ratio: Applications in Atmospheric Corrosion Studies. *Journal of the*

604   *Electrochemical Society, 163*(6), C316-C323. doi:10.1149/2.0751606jes

605   Emmons, L. K., Schwantes, R. H., Orlando, J. J., Tyndall, G., Kinnison, D., Lamarque, J. F., . . .

606   Pétron, G. (2020). The Chemistry Mechanism in the Community Earth System Model Version 2

607   (CESM2). *Journal of Advances in Modeling Earth Systems, 12*(4), 1-21.

608   doi:10.1029/2019ms001882

609   Emmons, L. K., Walters, S., Hess, P. G., Lamarque, J. F., Pfister, G. G., Fillmore, D., . . .

610   Kloster, S. (2010). Description and evaluation of the Model for Ozone and Related chemical

611   Tracers, version 4 (MOZART-4). *Geoscientific Model Development, 3*(1), 43-67.

612   doi:10.5194/gmd-3-43-2010

613   Faloona, I. (2009). Sulfur processing in the marine atmospheric boundary layer: A review and

614   critical assessment of modeling uncertainties. *Atmospheric Environment, 43*(18), 2841-2854.

615   doi:10.1016/j.atmosenv.2009.02.043

616   Fedkin, N. M., Li, C., Dickerson, R. R., Canty, T., & Krotkov, N. A. (2019). Linking

617   improvements in sulfur dioxide emissions to decreasing sulfate wet deposition by combining

618   satellite and surface observations with trajectory analysis. *Atmospheric Environment, 199*, 210-

619   223. doi:10.1016/j.atmosenv.2018.11.039

620   Feng, J., Vet, R., Cole, A., Zhang, L., Cheng, I., O'Brien, J., & Macdonald, A.-M. (2021).

621   Inorganic chemical components in precipitation in the eastern US and Eastern Canada during

622   1989-2016: Temporal and regional trends of wet concentration and wet deposition from the

623   NADP and CAPMoN measurements. *Atmospheric Environment, 254*.

624   doi:10.1016/j.atmosenv.2021.118367

625   Feng, L., Smith, S. J., Braun, C., Crippa, M., Gidden, M. J., Hoesly, R., . . . van der Werf, G. R.

626   (2020). The generation of gridded emissions data for CMIP6. *Geoscientific Model Development,*

627   *13*(2), 461-482. doi:10.5194/gmd-13-461-2020

628   Fioletov, V. E., McLinden, C. A., Krotkov, N., Li, C., Joiner, J., Theys, N., . . . Moran, M. D.

629   (2016). A global catalogue of large SO_2 sources and emissions derived from the Ozone

630   Monitoring Instrument. *Atmospheric Chemistry and Physics, 16*(18), 11497-11519.

631   doi:10.5194/acp-16-11497-2016

632 Flanner, M. G., Gardner, A. S., Eckhardt, S., Stohl, A., & Perket, J. (2014). Aerosol radiative

633 forcing from the 2010 Eyjafjallajokull volcanic eruptions. *Journal of Geophysical Research-*

634 *Atmospheres, 119*(15), 9481-9491. doi:10.1002/2014jd021977

635 Gao, M., Carmichael, G. R., Wang, Y., Ji, D., Liu, Z., & Wang, Z. (2016). Improving

636 simulations of sulfate aerosols during winter haze over Northern China: the impacts of

637 heterogeneous oxidation by NO_2. *Frontiers of Environmental Science & Engineering, 10*(5).

638 doi:10.1007/s11783-016-0878-2

639 Ge, W., Liu, J., Yi, K., Xu, J., Zhang, Y., Hu, X., . . . Tao, S. (2021). Influence of atmospheric

640 in-cloud aqueous-phase chemistry on the global simulation of SO_2 in CESM2. *Atmos. Chem.*

641 *Phys., 21*(21), 16093-16120. doi:10.5194/acp-21-16093-2021

642 Gelaro, R., McCarty, W., Suarez, M. J., Todling, R., Molod, A., Takacs, L., . . . Zhao, B. (2017).

643 The Modern-Era Retrospective Analysis for Research and Applications, Version 2 (MERRA-2).

644 *Journal of Climate, 30*(14), 5419-5454. doi:10.1175/jcli-d-16-0758.1

645 Geng, G., Xiao, Q., Zheng, Y., Tong, D., Zhang, Y., Zhang, X., . . . Liu, Y. (2019). Impact of

646 China's Air Pollution Prevention and Control Action Plan on $PM_{2.5}$ chemical composition over

647 eastern China. *Science China-Earth Sciences, 62*(12), 1872-1884. doi:10.1007/s11430-018-9353-

648 x

649 Georgiou, G. K., Christoudias, T., Proestos, Y., Kushta, J., Hadjinicolaou, P., & Lelieveld, J.

650 (2018). Air quality modelling in the summer over the eastern Mediterranean using WRF-Chem:

651 chemistry and aerosol mechanism intercomparison. *Atmospheric Chemistry and Physics, 18*(3),

652 1555-1571. doi:10.5194/acp-18-1555-2018

653   Goto, D., Nakajima, T., Takemura, T., & Sudo, K. (2011). A study of uncertainties in the sulfate

654   distribution and its radiative forcing associated with sulfur chemistry in a global aerosol model.

655   *Atmospheric Chemistry and Physics, 11*(21), 10889-10910. doi:10.5194/acp-11-10889-2011

656   Green, J. R., Fiddler, M. N., Holloway, J. S., Fibiger, D. L., McDuffie, E. E., Campuzano-Jost,

657   P., . . . Brown, S. S. (2019). Rates of Wintertime Atmospheric SO_2 Oxidation based on Aircraft

658   Observations during Clear-Sky Conditions over the Eastern United States. *Journal of*

659   *Geophysical Research-Atmospheres, 124*(12), 6630-6649. doi:10.1029/2018jd030086

660   Haywood, J. M., & Ramaswamy, V. (1998). Global sensitivity studies of the direct radiative

661   forcing due to anthropogenic sulfate and black carbon aerosols. *Journal of Geophysical*

662   *Research-Atmospheres, 103*(D6), 6043-6058. doi:10.1029/97jd03426

663   Hoesly, R. M., Smith, S. J., Feng, L., Klimont, Z., Janssens-Maenhout, G., Pitkanen, T., . . .

664   Zhang, Q. (2018). Historical (1750-2014) anthropogenic emissions of reactive gases and aerosols

665   from the Community Emissions Data System (CEDS). *Geoscientific Model Development, 11*(1),

666   369-408. doi:10.5194/gmd-11-369-2018

667   Horowitz, L. W. (2006). Past, present, and future concentrations of tropospheric ozone and

668   aerosols: Methodology, ozone evaluation, and sensitivity to aerosol wet removal. *Journal of*

669   *Geophysical Research-Atmospheres, 111*(D22). doi:10.1029/2005jd006937

670   Huang, L., An, J., Koo, B., Yarwood, G., Yan, R., Wang, Y., . . . Li, L. (2019). Sulfate formation

671   during heavy winter haze events and the potential contribution from heterogeneous $SO_2 + NO_2$

672   reactions in the Yangtze River Delta region, China. *Atmospheric Chemistry and Physics, 19*(22),

673   14311-14328. doi:10.5194/acp-19-14311-2019

674 Huang, X., Song, Y., Zhao, C., Li, M., Zhu, T., Zhang, Q., & Zhang, X. (2014). Pathways of
675 sulfate enhancement by natural and anthropogenic mineral aerosols in China. *Journal of*
676 *Geophysical Research-Atmospheres, 119*(24), 14165-14179. doi:10.1002/2014jd022301

677 Hussain, R., & Lun, K. (2019). The Geological Availability and Emissions of Sulfur and SO_2
678 from the Typical Coal of China. *Aerosol and Air Quality Research, 19*(3), 559-570.
679 doi:10.4209/aaqr.2018.08.0281

680 Intergovernmental Panel on Climate, C. (2014). *Climate Change 2013 – The Physical Science*
681 *Basis: Working Group I Contribution to the Fifth Assessment Report of the Intergovernmental*
682 *Panel on Climate Change*. Cambridge: Cambridge University Press.

683 Itahashi, S. (2018). Toward Synchronous Evaluation of Source Apportionments for Atmospheric
684 Concentration and Deposition of Sulfate Aerosol Over East Asia. *Journal of Geophysical*
685 *Research-Atmospheres, 123*(5), 2927-2953. doi:10.1002/2017jd028110

686 Itahashi, S., Yumimoto, K., Uno, I., Hayami, H., Fujita, S.-i., Pan, Y., & Wang, Y. (2018). A 15-
687 year record (2001-2015) of the ratio of nitrate to non-sea-salt sulfate in precipitation over East
688 Asia. *Atmospheric Chemistry and Physics, 18*(4), 2835-2852. doi:10.5194/acp-18-2835-2018

689 Jo, Y.-J., Lee, H.-J., Jo, H.-Y., Woo, J.-H., Kim, Y., Lee, T., . . . Kim, C.-H. (2020). Changes in
690 inorganic aerosol compositions over the Yellow Sea area from impact of Chinese emissions
691 mitigation. *Atmospheric Research, 240*. doi:10.1016/j.atmosres.2020.104948

692 Karplus, V. J., Zhang, S., & Almond, D. (2018). Quantifying coal power plant responses to
693 tighter SO_2 emissions standards in China. *Proceedings of the National Academy of Sciences of*
694 *the United States of America, 115*(27), 7004-7009. doi:10.1073/pnas.1800605115

695 Kasoar, M., Voulgarakis, A., Lamarque, J.-F., Shindell, D. T., Bellouin, N., Collins, W. J., . . .
696 Tsigaridis, K. (2016). Regional and global temperature response to anthropogenic SO_2 emissions

697   from China in three climate models. *Atmospheric Chemistry and Physics, 16*(15), 9785-9804.

698   doi:10.5194/acp-16-9785-2016

699   Keene, W. C., Galloway, J. N., Likens, G. E., Deviney, F. A., Mikkelsen, K. N., Moody, J. L., &

700   Maben, J. R. (2015). Atmospheric Wet Deposition in Remote Regions: Benchmarks for

701   Environmental Change. *Journal of the Atmospheric Sciences, 72*(8), 2947-2978. doi:10.1175/jas-

702   d-14-0378.1

703   Kipling, Z., Stier, P., Johnson, C. E., Mann, G. W., Bellouin, N., Bauer, S. E., . . . Zhang, K.

704   (2016). What controls the vertical distribution of aerosol? Relationships between process

705   sensitivity in HadGEM3-UKCA and inter-model variation from AeroCom Phase II. *Atmospheric*

706   *Chemistry and Physics, 16*(4), 2221-2241. doi:10.5194/acp-16-2221-2016

707   Lamarque, J. F., Emmons, L. K., Hess, P. G., Kinnison, D. E., Tilmes, S., Vitt, F., . . . Tyndall,

708   G. K. (2012). CAM-chem: description and evaluation of interactive atmospheric chemistry in the

709   Community Earth System Model. *Geoscientific Model Development, 5*(2), 369-411.

710   doi:10.5194/gmd-5-369-2012

711   Lee, H.-J., Jo, H.-Y., Song, C.-K., Jo, Y.-J., Park, S.-Y., & Kim, C.-H. (2020). Sensitivity of

712   Simulated $PM_{2.5}$ Concentrations over Northeast Asia to Different Secondary Organic Aerosol

713   Modules during the KORUS-AQ Campaign. *Atmosphere, 11*(9). doi:10.3390/atmos11091004

714   Li, B., Gasser, T., Ciais, P., Piao, S., Tao, S., Balkanski, Y., . . . Zhou, F. (2016). The

715   contribution of China's emissions to global climate forcing. *Nature, 531*(7594), 357-+.

716   doi:10.1038/nature17165

717   Li, B., Wang, X., Lei, R., Li, X., Li, W., & Fu, B. (2018). Numerical Simulation of Sulfate and

718   Black Carbon Pollution in East Asia. [东亚硫酸盐及黑碳污染特征数值模拟]. *Environmental*

719   *Science and Technology, 41*(5), 138-145. Retrieved from <u><Go to ISI>://CSCD:6257438</u>

720   Li, G., Bei, N., Cao, J., Huang, R., Wu, J., Feng, T., . . . Molina, L. T. (2017). A possible

721   pathway for rapid growth of sulfate during haze days in China. *Atmospheric Chemistry and*

722   *Physics, 17*(5), 3301-3316. doi:10.5194/acp-17-3301-2017

723   Li, H., Cheng, J., Zhang, Q., Zheng, B., Zhang, Y., Zheng, G., & He, K. (2019). Rapid transition

724   in winter aerosol composition in Beijing from 2014 to 2017: response to clean air actions.

725   *Atmospheric Chemistry and Physics, 19*(17), 11485-11499. doi:10.5194/acp-19-11485-2019

726   Li, J., Zhang, Y.-L., Cao, F., Zhang, W., Fan, M., Lee, X., & Michalski, G. (2020). Stable Sulfur

727   Isotopes Revealed a Major Role of Transition-Metal Ion-Catalyzed SO_2 Oxidation in Haze

728   Episodes. *Environmental Science & Technology, 54*(5), 2626-2634. doi:10.1021/acs.est.9b07150

729   Li, X., & Liu, Y. (2013). Assessment of Two Aerosol Modules of CAM5. [Cam5 模式中两气溶

730   胶模块的评估]. *Journal of Applied Meteorolgical Science, 24*(1), 75-86. Retrieved from <u><Go to</u>

731   <u>ISI>://CSCD:4771081</u>

732   Li, X., Zhao, B., Zhou, W., Shi, H., Yin, R., Cai, R., . . . Jiang, J. (2020). Responses of gaseous

733   sulfuric acid and particulate sulfate to reduced SO_2 concentration: A perspective from long-term

734   measurements in Beijing. *Science of the Total Environment, 721*.

735   doi:10.1016/j.scitotenv.2020.137700

736   Liu, B., Wu, J., Zhang, J., Wang, L., Yang, J., Liang, D., . . . Zhang, Q. (2017). Characterization

737   and source apportionment of $PM_{2.5}$ based on error estimation from EPA PMF 5.0 model at a

738   medium city in China. *Environmental Pollution, 222*, 10-22. doi:10.1016/j.envpol.2017.01.005

739   Liu, J., Fan, S., Horowitz, L. W., & Levy, H., II. (2011). Evaluation of factors controlling long-

740   range transport of black carbon to the Arctic. *Journal of Geophysical Research-Atmospheres,*

741   *116*. doi:10.1029/2010jd015145

742 Liu, L., Shawki, D., Voulgarakis, A., Kasoar, M., Samset, B. H., Myhre, G., . . . Takemura, T.
743 (2018). A PDRMIP Multimodel Study on the Impacts of Regional Aerosol Forcings on Global
744 and Regional Precipitation. *Journal of Climate, 31*(11), 4429-4447. doi:10.1175/jcli-d-17-0439.1

745 Liu, M., & Matsui, H. (2021). Aerosol radiative forcings induced by substantial changes in
746 anthropogenic emissions in China from 2008 to 2016. *Atmospheric Chemistry and Physics,*
747 *21*(8), 5965-5982. doi:10.5194/acp-21-5965-2021

748 Liu, M., Song, Y., Xu, T., Xu, Z., Wang, T., Yin, L., . . . Tang, J. (2020). Trends of Precipitation
749 Acidification and Determining Factors in China During 2006-2015. *Journal of Geophysical*
750 *Research-Atmospheres, 125*(6). doi:10.1029/2019jd031301

751 Liu, X., Easter, R. C., Ghan, S. J., Zaveri, R., Rasch, P., Shi, X., . . . Mitchell, D. (2012). Toward
752 a minimal representation of aerosols in climate models: description and evaluation in the
753 Community Atmosphere Model CAM5. *Geoscientific Model Development, 5*(3), 709-739.
754 doi:10.5194/gmd-5-709-2012

755 Liu, X., Penner, J. E., Das, B., Bergmann, D., Rodriguez, J. M., Strahan, S., . . . Feng, Y. (2007).
756 Uncertainties in global aerosol simulations: Assessment using three meteorological data sets.
757 *Journal of Geophysical Research-Atmospheres, 112*(D11). doi:10.1029/2006jd008216

758 Lu, X., Fung, J. C. H., & Wu, D. (2015). Modeling wet deposition of acid substances over the
759 PRD region in China. *Atmospheric Environment, 122*, 819-828.
760 doi:10.1016/j.atmosenv.2015.09.035

761 Luo, G., Yu, F., & Moch, J. M. (2020). Further improvement of wet process treatments in
762 GEOS-Chem v12.6.0: impact on global distributions of aerosols and aerosol precursors.
763 *Geoscientific Model Development, 13*(6), 2879-2903. doi:10.5194/gmd-13-2879-2020

Ma, X.-x., Liu, H.-n., Wang, X.-y., & Zhang, R.-j. (2016). THE RADIATIVE EFFECTS OF ANTHROPOGENIC AEROSOLS OVER CHINA AND THEIR SENSITIVITY TO SOURCE EMISSION. *Journal of Tropical Meteorology, 22*(1), 94-108. Retrieved from <u><Go to ISI>://WOS:000371651900011</u>

Ma, X., Shi, G., Guo, Y., & Wang, X. (2005). RADIATIVE FORCING BY GREENHOUSE GASES AND SULFATE AEROSOL. [温室气体和硫酸盐气溶胶的辐射强迫作用]. *Acta Meteorologica Sinica, 63*(1), 41-48. Retrieved from <u><Go to ISI>://CSCD:1868240</u>

Matus, A. V., L'Ecuyer, T. S., & Henderson, D. S. (2019). New Estimates of Aerosol Direct Radiative Effects and Forcing From A-Train Satellite Observations. *Geophysical Research Letters, 46*(14), 8338-8346. doi:10.1029/2019gl083656

McClure, C. D., & Jaffe, D. A. (2018). US particulate matter air quality improves except in wildfire-prone areas. *Proceedings of the National Academy of Sciences of the United States of America, 115*(31), 7901-7906. doi:10.1073/pnas.1804353115

McDuffie, E. E., Smith, S. J., O'Rourke, P., Tibrewal, K., Venkataraman, C., Marais, E. A., . . . Martin, R. V. (2020). A global anthropogenic emission inventory of atmospheric pollutants from sector- and fuel-specific sources (1970-2017): an application of the Community Emissions Data System (CEDS). *Earth System Science Data, 12*(4), 3413-3442. doi:10.5194/essd-12-3413-2020

Ming, Y., Ramaswamy, V., Ginoux, P. A., Horowitz, L. W., & Russell, L. M. (2005). Geophysical Fluid Dynamics Laboratory general circulation model investigation of the indirect radiative effects of anthropogenic sulfate aerosol. *Journal of Geophysical Research-Atmospheres, 110*(D22). doi:10.1029/2005jd006161

785   Molod, A., Takacs, L., Suarez, M., & Bacmeister, J. (2015). Development of the GEOS-5

786   atmospheric general circulation model: evolution from MERRA to MERRA2. *Geoscientific*

787   *Model Development, 8*(5), 1339-1356. doi:10.5194/gmd-8-1339-2015

788   Ni, M., Zheng, J., Ma, Y., Wang, L., & Wang, M. (2016). Research Progress in Radiative

789   Forcing of Aerosol. [气溶胶的辐射强迫作用研究进展]. *Environmental Science and*

790   *Technology, 39*(10), 73-78,112. Retrieved from <u><Go to ISI>://CSCD:5856358</u>

791   Paulot, F., Paynter, D., Ginoux, P., Naik, V., & Horowitz, L. W. (2018). Changes in the aerosol

792   direct radiative forcing from 2001 to 2015: observational constraints and regional mechanisms.

793   *Atmospheric Chemistry and Physics, 18*(17), 13265-13281. doi:10.5194/acp-18-13265-2018

794   Penner, J. E., Chuang, C. C., & Grant, K. (1998). Climate forcing by carbonaceous and sulfate

795   aerosols. *Climate Dynamics, 14*(12), 839-851. doi:10.1007/s003820050259

796   Qiao, X., Xiao, W., Jaffe, D., Kota, S. H., Ying, Q., & Tang, Y. (2015). Atmospheric wet

797   deposition of sulfur and nitrogen in Jiuzhaigou National Nature Reserve, Sichuan Province,

798   China. *Science of the Total Environment, 511*, 28-36. doi:10.1016/j.scitotenv.2014.12.028

799   Richardson, T. B., Forster, P. M., Smith, C. J., Maycock, A. C., Wood, T., Andrews, T., . . .

800   Watson-Parris, D. (2019). Efficacy of Climate Forcings in PDRMIP Models. *Journal of*

801   *Geophysical Research-Atmospheres, 124*(23), 12824-12844. doi:10.1029/2019jd030581

802   Rogora, M., Colombo, L., Marchetto, A., Mosello, R., & Steingruber, S. (2016). Temporal and

803   spatial patterns in the chemistry of wet deposition in Southern Alps. *Atmospheric Environment,*

804   *146*, 44-54. doi:10.1016/j.atmosenv.2016.06.025

805   Sanchez, K. J., Chen, C.-L., Russell, L. M., Betha, R., Liu, J., Price, D. J., . . . Behrenfeld, M. J.

806   (2018). Substantial Seasonal Contribution of Observed Biogenic Sulfate Particles to Cloud

807   Condensation Nuclei. *Scientific Reports, 8*. doi:10.1038/s41598-018-21590-9

808   Sedefian, L., Ku, M., Civerolo, K., Hao, W., & Zalewsky, E. (2016, Oct 03-07, 2018). *Regional*

809   *Refined Grid Modeling of Acidic and Mercury Deposition over Northeastern US and the*

810   *Contribution of New York Power Point Sources.* Paper presented at the 35th International

811   Technical Meeting on Air Pollution Modelling and its Application (ITM), Chania, GREECE.

812   Sha, T., Ma, X., Jia, H., Tian, R., Chang, Y., Cao, F., & Zhang, Y. (2019). Aerosol chemical

813   component: Simulations with WRF-Chem and comparison with observations in Nanjing.

814   *Atmospheric Environment, 218*. doi:10.1016/j.atmosenv.2019.116982

815   Shao, J., Chen, Q., Wang, Y., Lu, X., He, P., Sun, Y., . . . Alexander, B. (2019). Heterogeneous

816   sulfate aerosol formation mechanisms during wintertime Chinese haze events: air quality model

817   assessment using observations of sulfate oxygen isotopes in Beijing. *Atmospheric Chemistry and*

818   *Physics, 19*(9), 6107-6123. doi:10.5194/acp-19-6107-2019

819   Shawki, D., Voulgarakis, A., Chakraborty, A., Kasoar, M., & Srinivasan, J. (2018). The South

820   Asian Monsoon Response to Remote Aerosols: Global and Regional Mechanisms. *Journal of*

821   *Geophysical Research-Atmospheres, 123*(20), 11585-11601. doi:10.1029/2018jd028623

822   Sickles, J. E., II, & Shadwick, D. S. (2015). Air quality and atmospheric deposition in the eastern

823   US: 20 years of change. *Atmospheric Chemistry and Physics, 15*(1), 173-197. doi:10.5194/acp-

824   15-173-2015

825   Smith, C. J., Kramer, R. J., Myhre, G., Alterskjaer, K., Collins, W., Sima, A., . . . Forster, P. M.

826   (2020). Effective radiative forcing and adjustments in CMIP6 models. *Atmospheric Chemistry*

827   *and Physics, 20*(16), 9591-9618. doi:10.5194/acp-20-9591-2020

828   Sobhani, N., Kulkarni, S., & Carmichael, G. R. (2018). Source sector and region contributions to

829   black carbon and $PM_{2.5}$ in the Arctic. *Atmospheric Chemistry and Physics, 18*(24), 18123-18148.

830   doi:10.5194/acp-18-18123-2018

831   Steven, J. S., Yuyu, Z., & Page, K. (2015). *A Community Emissions Data System (CEDS)*

832   *Emissions For CMIP6 and Beyond*. Paper presented at the 2015 International Emission

833   Inventory Conference, San Diego, CA.

834   Stevens, B. (2015). Rethinking the Lower Bound on Aerosol Radiative Forcing. *Journal of*

835   *Climate, 28*(12), 4794-4819. doi:10.1175/jcli-d-14-00656.1

836   Thornhill, G. D., Collins, W. J., Kramer, R. J., Olivi, D., Skeie, R. B., O'Connor, F. M., . . .

837   Zhang, J. (2021). Effective radiative forcing from emissions of reactive gases and aerosols - a

838   multi-model comparison. *Atmospheric Chemistry and Physics, 21*(2), 853-874. doi:10.5194/acp-

839   21-853-2021

840   Vivanco, M. G., Bessagnet, B., Cuvelier, C., Theobald, M. R., Tsyro, S., Pirovano, G., . . . Ung,

841   A. (2017). Joint analysis of deposition fluxes and atmospheric concentrations of inorganic

842   nitrogen and sulphur compounds predicted by six chemistry transport models in the frame of the

843   EURODELTAIII   project.   *Atmospheric   Environment,   151*,   152-175.

844   doi:10.1016/j.atmosenv.2016.11.042

845   Wang, W., Liu, M., Wang, T., Song, Y., Zhou, L., Cao, J., . . . Ge, M. (2021). Sulfate formation

846   is dominated by manganese-catalyzed oxidation of SO_2 on aerosol surfaces during haze events.

847   *Nature Communications, 12*(1). doi:10.1038/s41467-021-22091-6

848   Wei, Y., Chen, X., Chen, H., Li, J., Wang, Z., Yang, W., . . . Huang, H. (2019). IAP-AACM

849   v1.0: a global to regional evaluation of the atmospheric chemistry model in CAS-ESM.

850   *Atmospheric Chemistry and Physics, 19*(12), 8269-8296. doi:10.5194/acp-19-8269-2019

851   Wofsy, S. C., Afshar, S., Allen, H. M., Apel, E. C., Asher, E. C., Barletta, B., . . . Vieznor, N.

852   (2021). ATom: Merged Atmospheric Chemistry, Trace Gases, and Aerosols, Version 2. In:

853   ORNL Distributed Active Archive Center.

854   Wu, T., Zhang, F., Zhang, J., Jie, W., Zhang, Y., Wu, F., . . . Hu, A. (2020). Beijing Climate

855   Center Earth System Model version 1 (BCC-ESM1): model description and evaluation of aerosol

856   simulations. *Geoscientific Model Development, 13*(3), 977-1005. doi:10.5194/gmd-13-977-2020

857   Xie, X., Liu, X., Wang, H., & Wang, Z. (2016). Effects of Aerosols on Radiative Forcing and

858   Climate Over East Asia With Different SO_2 Emissions. *Atmosphere, 7*(8).

859   doi:10.3390/atmos7080099

860   Xue, J., Yuan, Z., Griffith, S. M., Yu, X., Lau, A. K. H., & Yu, J. Z. (2016). Sulfate Formation

861   Enhanced by a Cocktail of High NO_x, SO_2, Particulate Matter, and Droplet pH during Haze-Fog

862   Events in Megacities in China: An Observation-Based Modeling Investigation. *Environmental*

863   *Science & Technology, 50*(14), 7325-7334. doi:10.1021/acs.est.6b00768

864   Yan, X., & Xu, Y. (2021). SO_2 mitigation in China's coal-fired power plants: A satellite-based

865   assessment on compliance and enforcement. *Atmospheric Environment, 254*.

866   doi:10.1016/j.atmosenv.2021.118396

867   Yang, Y., Wang, H., Smith, S. J., Easter, R., Ma, P.-L., Qian, Y., . . . Rasch, P. J. (2017). Global

868   source attribution of sulfate concentration and direct and indirect radiative forcing. *Atmospheric*

869   *Chemistry and Physics, 17*(14), 8903-8922. doi:10.5194/acp-17-8903-2017

870   Yang, Y., Wang, H., Smith, S. J., Easter, R. C., & Rasch, P. J. (2018). Sulfate Aerosol in the

871   Arctic: Source Attribution and Radiative Forcing. *Journal of Geophysical Research-*

872   *Atmospheres, 123*(3), 1899-1918. doi:10.1002/2017jd027298

873   Yue, F., Xie, Z., Zhang, P., Song, S., He, P., Liu, C., . . . Kang, H. (2019). The role of sulfate and

874   its corresponding S(IV)+NO_2 formation pathway during the evolution of haze in Beijing. *Science*

875   *of the Total Environment, 687*, 741-751. doi:10.1016/j.scitotenv.2019.06.096

876 Zhang, B., Zhou, T., Liu, Y., Yan, C., Li, X., Yu, J., . . . Zheng, M. (2019). Comparison of water-

877 soluble inorganic ions and trace metals in $PM_{2.5}$ between online and offline measurements in

878 Beijing during winter. *Atmospheric Pollution Research, 10*(6), 1755-1765.

879 doi:10.1016/j.apr.2019.07.007

880 Zhang, F., Wang, Y., Peng, J., Chen, L., Sun, Y., Duan, L., . . . Zhang, R. (2020). An unexpected

881 catalyst dominates formation and radiative forcing of regional haze. *Proceedings of the National*

882 *Academy of Sciences of the United States of America, 117*(8), 3960-3966.

883 doi:10.1073/pnas.1919343117

884 Zhang, H., & Huang, J. (2014). Interpretation of the IPCC Fifth Assessment Report on

885 Anthropogenic and Natural Radiative Forcing. *Advances in Climate Change Research, 10*(1), 40-

886 44. doi:10.3969/j.issn.1673-1719.2014.01.009

887 Zheng, B., Zhang, Q., Zhang, Y., He, K. B., Wang, K., Zheng, G. J., . . . Kimoto, T. (2015).

888 Heterogeneous chemistry: a mechanism missing in current models to explain secondary

889 inorganic aerosol formation during the January 2013 haze episode in North China. *Atmospheric*

890 *Chemistry and Physics, 15*(4), 2031-2049. doi:10.5194/acp-15-2031-2015

891 Zheng, H., Song, S., Sarwar, G., Gen, M., Wang, S., Ding, D., . . . McElroy, M. B. (2020).

892 Contribution of Particulate Nitrate Photolysis to Heterogeneous Sulfate Formation for Winter

893 Haze in China. *Environmental Science & Technology Letters, 7*(9), 632-638.

894 doi:10.1021/acs.estlett.0c00368

895 Zheng, K., Zhao, T., Zhang, L., Zeng, N., Zheng, X., & Yang, Q. (2019). Characteristics of Wet

896 Deposition of Sulfate and Nitrate in Three Typical Cities in China in 2001-2017. [2001-2017 年

897 中国 3 个典型城市硫酸盐和硝酸盐湿沉降特征]. *Ecology and Environmental Sciences,*

898 *28*(12), 2390-2397. Retrieved from <Go to ISI>://CSCD:6643937

899   Zhou, S., Wu, L., Guo, J., Chen, W., Wang, X., Zhao, J., . . . Kuang, J. (2020). Measurement

900   report: Vertical distribution of atmospheric particulate matter within the urban boundary layer in

901   southern China - size-segregated chemical composition and secondary formation through cloud

902   processing and heterogeneous reactions. *Atmospheric Chemistry and Physics, 20*(11), 6435-

903   6453. doi:10.5194/acp-20-6435-2020

904